Accurate holographic imaging of colloidal particle pairs by Rayleigh-Sommerfeld reconstruction

David Kapfenberger,[1] **Adar Sonn-Segev,**[2] **and Yael Roichman**[2,*]

[1]*School of Physics, Tel Aviv University, Tel Aviv 69978, Israel*
[2]*Raymond and Beverly Sackler School of Chemistry, Tel Aviv University, Tel Aviv 69978, Israel*
[*]*roichman@tau.ac.il*

Abstract: In-line holographic optical imaging has the unique capability of high speed imaging in three dimensions at rates limited only by the imaging rate of the camera used. In this technique the 3D data is recorded on the detector in a form of a hologram generated by diffraction between the scattered and unscattered light passing through the sample. For dilute samples of single particles or a small cluster of particles, this technique was shown to result in particle tracking with spatial positioning accuracy of a few nanometers. For dense suspension only approximate reconstruction were achieved with systematic axial positioning errors. We propose a scheme to extend accurate holographic microscopy to dense suspensions, by calibrating the Rayleigh-Sommerfeld reconstruction algorithm against Lorentz-Mie scattering theory. We perform this calibration both numerically and experimentally and define the parameter space in which accurate imaging is achieved, and in which numerical calibration holds. We demonstrate the validity of our approach by imaging two attached particles and measuring the distance between their centers with 36 nm accuracy. A difference of 50 nm in particle diameter is easily measured.

OCIS codes: (090.1760) Computer holography; (180.6900) Three-dimensional microscopy; (120.0120) Instrumentation, measurement, and metrology, (100.3010) Image reconstruction techniques.

References and links

1. G. Bolognesi, S. Bianchi, and R. D. Leonardo, "Digital holographic tracking of microprobes for multipoint viscosity measurements," Opt. Express **19**, 19245–19254 (2011).
2. J. Garcia-Sucerquia, W. Xu, S. K. Jericho, P. Klages, M. H. Jericho, and H. J. Kreuzer, "Digital in-line holographic microscopy," Appl. Opt. **45**, 836–850 (2006).
3. W. Xu, M. H. Jericho, H. J. Kreuzer, and I. A. Meinertzhagen, "Tracking particles in four dimensions with in-line holographic microscopy," Opt. Lett. **28**, 164–166 (2003).
4. L. Dixon, F. C. Cheong, and D. G. Grier, "Holographic deconvolution microscopy for high-resolution particle tracking," Opt. Express **19**, 16410–16417 (2011).
5. J. Sheng, E. Malkiel, and J. Katz, "Digital holographic microscope for measuring three-dimensional particle distributions and motions," Appl. Opt. **45**, 3893–3901 (2006).
6. F. C. Cheong, B. J. Krishnatreya, and D. G. Grier, "Strategies for three-dimensional particle tracking with holographic video microscopy," Opt. Express **18**, 13563–13573 (2010).
7. J. Fung, K. E. Martin, R. W. Perry, D. M. Kaz, R. McGorty, and V. N. Manoharan, "Measuring translational, rotational, and vibrational dynamics in colloids with digital holographic microscopy," Opt. Express **19**, 8051–8065 (2011).

#181894 - $15.00 USD Received 18 Dec 2012; revised 1 Mar 2013; accepted 5 Mar 2013; published 10 May 2013

8. F. C. Cheong and D. G. Grier, "Rotational and translational diffusion of copper oxide nanorods measured with holographic video microscopy," Opt. Express **18**, 6555–6562 (2010).
9. J. C. Crocker and D. G. Grier, "Methods of digital video microscopy for colloidal studies," J. Colloid Interface Sci. **179**, 298 – 310 (1996).
10. Y.-S. Choi and S.-J. Lee, "High-accuracy three-dimensional position measurement of tens of micrometers size transparent microspheres using digital in-line holographic microscopy," Opt. Lett. **36**, 4167–4169 (2011).
11. L. Cavallini, G. Bolognesi, and R. D. Leonardo, "Real-time digital holographic microscopy of multiple and arbitrarily oriented planes," Opt. Lett. **36**, 3491–3493 (2011).
12. T. Savin and P. S. Doyle, "Role of a finite exposure time on measuring an elastic modulus using microrheology," Phys. Rev. E **71**, 041106 (2005).
13. J. Goodman, *Introduction to Fourier Optics* (McGraw-Hill, 2005).
14. S.-H. Lee and D. G. Grier, "Holographic microscopy of holographically trapped three-dimensional structures," Opt. Express **15**, 1505–1512 (2007).
15. Y. Roichman, I. Cholis, and D. G. Grier, "Volumetric imaging of holographic optical traps," Opt. Express **14**, 10907–10912 (2006).
16. S. D. A. Russel, W. B. and W. R. Schowalter, *Colloidal Dispersions* (Cambridge University Press, 1989).

1. Introduction

Fast three dimensional imaging of dense microscopic colloidal suspensions is greatly desired for many applications, such as 3D fluid velocity field characterization, microrheology of complex media, and characterization of active motion in live cells. The most common microscopy technique used for three dimensional imaging is confocal microscopy, in which fluorescently labeled tracer particles are followed and tracked. The rate of imaging of the full field of view is determined by the camera capture rate, the fluorescence efficiency, and the number of planes imaged in the axial direction. In-line digital holographic microscopy is an imaging technique offering three dimensional imaging of unlabeled particle suspensions at a single camera exposure, capable of reaching kHz imaging rates in 3D [1, 2, 3]. However, accurate rendering of particle location within the sample, done in the framework of the Lorentz-Mie scattering theory, is restricted to very dilute samples having non-ovelapping diffraction patterns. Here we demonstrate how to extend accurate in-line holographic 3D positioning to denser suspensions.

Digital holographic microscopy (DHM) is a 3D imaging technique based on recording the interference pattern between a reference beam and a beam diffracted by a sample. This interference pattern constitutes a hologram that encodes the three dimensional image of the sample. In-line digital holography is a variant of the technique that uses the light that does not scatter by the sample as a reference beam. Since the reference beam and the scattered beam travel through exactly the same optical path except for diffracting from an imaged particle, the method is less sensitive to variations in refractive index,thickness, and composition. The implementation of in-line holographic microscopy involves replacing the bright field illumination of an optical microscope by collimated laser light. Two different approaches can be used to extract 3D particle positions from the obtained holograms, one based on reconstructing the hologram digitally, using Fresnel or Rayleigh-Sommerfeld diffraction integrals [2, 4, 5], and the other, by fitting the acquired diffraction pattern to the theoretical pattern calculated using Mie scattering and T-Matrix theory [6, 1, 7]. The most accurate method to date is the latter, based on fitting of the scattering data to the Mie scattering pattern of a single sphere [8], or to a superposition of them [5], achieving positioning accuracy as good as 7 nm laterally and 10 nm axially [4]. The normalized intensity on a plane perpendicular to the optical axis in such a hologram, is a function of the sphere's 3D position, size, refractive index and the refractive index of its environment [6]. When determining the laser's wavelength and the effective magnification, this fitting process yields a precise measure to the sphere's parameters and reveals more information than do hologram reconstruction algorithms. Once the 3D position of the particle is determined standard tracking algorithms [9] can be applied to characterize its motion. The main caveat of this fitting method is its sensitivity to imaging noise, overlapping diffraction patterns prevent

#181894 - $15.00 USD Received 18 Dec 2012; revised 1 Mar 2013; accepted 5 Mar 2013; published 10 May 2013

its convergence. As a result, accurate extraction of the three dimensional positions of particles is limited to very dilute suspension.

The Rayleigh-Sommerfeld reconstruction algorithm recreates the three dimensional light field producing the hologram without requiring prior knowledge of the sample shape and composition, enabling imaging of denser suspensions [6, 10, 4]. However, previous studies have shown that the extracted axial positions of beads in this method suffer from systematic errors whose extent depends on particle size, composition, and height [6]. In addition, axial positioning accuracy is reduced compared to Mie scattering fitting algorithms. Nontheless Rayleigh-Sommerfeld reconstruction has been used to follow diffusion of colloidal particles of various shapes [8, 4]. The more involved fitting procedure of the Lorentz-Mie approach requires intensive computation as compared with the straight forward back propagation of the Rayleigh-Sommerfeld reconstruction algorithm, which means that the Rayleigh-Sommerfeld scheme is easier to implement and faster to run by a factor depending on the specific implementation. This is not a major drawback however, since new implementations of Lorentz-Mie fitting, based on GPU accelerated protocols, enable real time analysis of in-line holographic data [11].

We propose a calibration scheme to correct for these axial positioning errors in order to achieve accurate 3D position rendering of dense colloidal suspensions within the Rayleigh-Sommerfeld reconstruction framework.In this study we identify the main sources of the systematic errors in the Rayleigh-Sommerfeld reconstruction algorithm and correct for them by calibrating the Rayleigh-Sommerfeld scheme against the Lorentz-Mie approach on simulated data, and on experimental data. As a result we achieve improved accuracy of 3D particle positioning using Rayleigh-Sommerfeld reconstruction. We proceed to demonstrate two scenarios in which the calibrated Rayleigh-Sommerfeld reconstruction produces better 3D particle positioning than the Lorentz-Mie approach; particles near a partially reflective wall, and two attached particles with overlapping diffraction patterns.

2. Rayleigh-Sommerfeld reconstruction

Rayleigh-Sommerfeld reconstruction of an in-line holographic microscope image involves three steps: Background subtraction, image back propagation, and image deconvolution [4]. Once the three dimensional image is obtained standard image analysis algorithms are used to identify feature locations, from which particle location is then interpreted. Let us describe the reference beam and scattered light in In-line microscopy following the notation of [6, 4] as:

$$\begin{aligned} \vec{E}_0(\vec{r},z) &= E_0(\vec{r})\, e^{ikz}\hat{\varepsilon}_0 \\ \vec{E}_s(\vec{r},z) &= E_s(\vec{r},z)\,\hat{\varepsilon}(\vec{r},z) \end{aligned} \tag{1}$$

were the incident illumination $\vec{E}_0(\vec{r},z)$ is assumed to be a plane wave propagating along $\hat{z}$ with wavenumber k. The interference between both beams creates a hologram on the detector with an intensity profile given by:

$$I(\vec{r}) = \left|\vec{E}_0(\vec{r},z)+\vec{E}_s(\vec{r},z)\right|^2 = E_0^2(\vec{r}) + 2Re\left\{E_0(\vec{r})\,E_s(\vec{r},z)\,\hat{\varepsilon}_0^*\cdot\hat{\varepsilon}(\vec{r},z)\right\} + \left|\vec{E}_s(\vec{r},z)\right|^2 \tag{2}$$

Moving the microscope's objective away from the scatterer places it well above the focal plane and ensures that polarization rotations are small, $\hat{\varepsilon}_0^*\cdot\hat{\varepsilon}(\vec{r},z)\approx 1$. For reconstruction purposes, the term $|E_S(\vec{r},0)|^2$ reflecting multiple scattering events is neglected as well [6]. Dividing the recorded hologram $I(\vec{r})$ by the illumination's intensity distribution $I_0(\vec{r}) = E_0^2(\vec{r})$ then yields:

$$b(\vec{r}) \equiv \frac{I(\vec{r})}{I_0}(\vec{r}) - 1 \approx 2Re\left\{E_S(\vec{r},0)\right\} \tag{3}$$

#181894 - $15.00 USD Received 18 Dec 2012; revised 1 Mar 2013; accepted 5 Mar 2013; published 10 May 2013

where the reduced scattered field is $E_S(\vec{r},z) = E_s(\vec{r},z)/E_0(\vec{r})$. Good estimations of the illumination background, $I_0(\vec{r})$, can be obtained by calculating the running median of the analyzed sequence. The positioning accuracy of the Rayleigh-Sommerfeld reconstruction algorithm depends, among other things, on the quality of background subtraction, and extent of optical noise. These errors can be estimated from a mean square displacement plot of a diffusing particle [12, 4]. Conventional accuracies measured in this manner range up to 20 nm laterally and 60 nm axially [4]. Once the hologram is recorded and normalized by its background, the scattered field at height z above the focal plane may be reconstructed from the complex field at the focal plane by convolving $E_S(\vec{r},0)$ with the the Rayleigh–Sommerfeld propagator $h(\vec{r},-z)$ [13]:

$$E_S(\vec{r},z) = E_S(\vec{r},0) \otimes h(\vec{r},-z) \tag{4}$$

where $h(\vec{r},-z) = \frac{1}{2\pi}\frac{\partial}{\partial z}\frac{e^{ikR}}{R}$, $R^2 = r^2 + z^2$, and positive sign of z refers to the distance above the focal plane towards the light source. This convolution can be approximated by:

$$E_S(\vec{r},z) \approx \frac{e^{-ikz}}{4\pi^2}\int_{-\infty}^{\infty} B(\vec{q})H(\vec{q},-z)e^{i\vec{q}\cdot\vec{r}}d^2\vec{q} \tag{5}$$

where $H(\vec{q},-z)$ and $B(\vec{q})$ are the Fourier transforms of $h(\vec{r},-z)$ and $b(\vec{r})$ respectively. The volumetric reconstruction intensity, $I_R(\vec{r},z) = |E_S(\vec{r},z)|^2$, is an approximate representation of the sample, suffering from artifacts of imaging and reconstruction [4]. Following Dixon *et al.* [4] we now deconvolve our volumetric reconstruction with the Rayleigh-Sommerfeld point spread function itself, $K_R(\vec{r},z-z_p) = \left|h(\vec{r},z-z_p)\right|^2$, in Fourier space:

$$\tilde{I}_D(\rho) = \frac{\tilde{I}_R(\rho)}{\tilde{K}(\rho)+\chi} \tag{6}$$

where $\tilde{I}_R(\rho)$ and $\tilde{K}(\rho)$ are the Fourier transforms of $I_R(\vec{r},z)$ and $K_R(\vec{r},z)$, respectively, and χ is a small factor chosen for numerical stability. The deconvolved intensity, $I_D(\vec{r},z)$ is obtained as the inverse Fourier transform of $\tilde{I}_D(\rho)$. Using deconvolution filtering reduces noise inducing effects such as twin image noise [4], resulting in a twofold improvement in positioning accuracy. A transparent colloidal particle subjected to plane wave illumination acts as an imperfect lens and focuses the light to a focal spot further away. The bright feature observed in the 3D light pattern reconstructed from a hologram is then identified as that focal spot. For large particles, of the order of 30 μm in diameter the distance between the focal spot and the particle can be calculated analytically, $f_{sphere} \sim \frac{a_p}{2}\left(\frac{n_m}{n_p - n_m}\right)$ and is in accord with experimental measurements [10]. However, previous studies have shown that the axial position of smaller colloidal particles, of the order of 1 μm, calculated by the Rayleigh-Sommerfeld reconstruction algorithm is shifted form the one obtained by fitting to Lorentz-Mie theory by an amount which depends not only on the refractive index of bead and suspension, and on bead size, but also on the bead's distance from the focal plane [6]. In the following section we will describe a calibration scheme that corrects for these errors rendering Rayleigh-Sommerfeld reconstruction accurate.

3. Calibrating Rayleigh-Sommerfeld reconstruction

3.1. Numerical calibration

We consider now the incident plane-wave and the scattered light from a spherical particle, $\vec{E}_0$ and $\vec{E}_s$, as defined in Eq. (1). We describe the scattered field at position $\vec{r}$ in the focal plane due to an object at $\vec{r_p}$, relative to the center of the focal plane, as [6]:

$$\vec{E}_s(\vec{r},0) = E_0(\vec{r_p})\vec{f}_s(k(\vec{r}-\vec{r_p})) \tag{7}$$

#181894 - $15.00 USD Received 18 Dec 2012; revised 1 Mar 2013; accepted 5 Mar 2013; published 10 May 2013

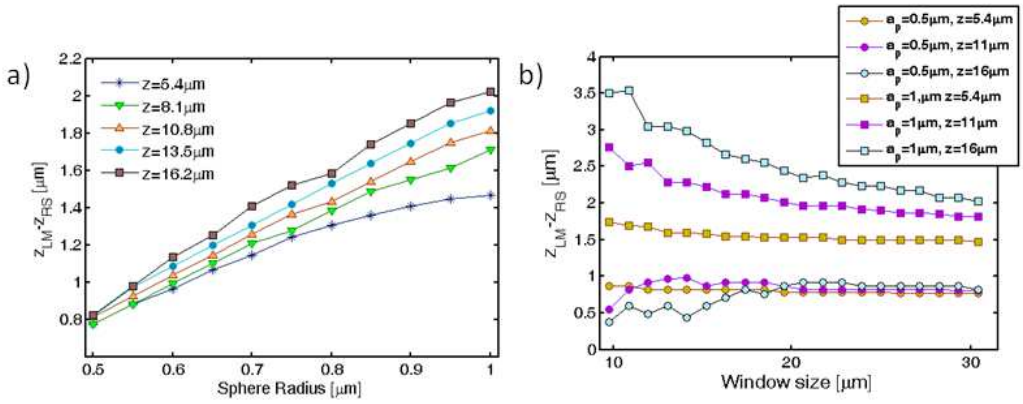

Fig. 1. Numerical calibration of Rayleigh-Sommerfeld reconstruction against Lorentz-Mie (LM) scattering theory. Calibration graph of polystyrene sphere's effective focal length $\Delta z = z_{LM} - z_{RS}$ in TE buffer, (a) as a function of the sphere's size, and (b) as a function of field0of-view size. The focal length varies across the sphere's height and is more significant for larger particles due to the decrease in the number of diffration ring in the field-of-view.

where $\vec{f}_s(k(\vec{r}-\vec{r_p}))$ is the field scattered from our particle, and given by [6]:

$$\vec{f}_s(k\vec{r}) = \sum_{n=1}^{n_c} \frac{i^n(2n+1)}{n(n+1)}[ia_n\vec{N}^{(3)}_{e1n}(k\vec{r}) - b_n\vec{M}^{(3)}_{o1n}(k\vec{r})] \tag{8}$$

according to Lorentz-Mie scattering theory. $\vec{M}^{(1)}_{o1n}$ and $\vec{N}^{(1)}_{e1n}$ are vector spherical harmonic functions of the first kind, their coefficients depending on the sphere's position, radius (a_p), refractive index (n_p) and the refractive index of its environment (n_m) [6]. With these definitions, the normalized hologram can be written as:

$$B(\vec{r}) \equiv \frac{I(\vec{r})}{I_0(\vec{r})} \approx 1 + 2Re\left\{\vec{f}_s(k(\vec{r}-\vec{r_p}))\cdot\hat{\varepsilon}_0\right\} + \left|\vec{f}_s(k(\vec{r}-\vec{r_p}))\right|^2 \tag{9}$$

Here we can use the full functional form of the scattered field. The Lorentz-Mie reconstruction protocol amounts, in practice, to fitting the experimentally obtained hologram to this analytical two dimensional function. Alternatively, the Lorentz-Mie theory can be used to simulate in-line holograms of a colloidal particle of given size, refractive index, and position, in a medium of choice.

In order to calibrate the Rayleigh-Sommerfeld scheme for hologram reconstruction, we first simulated theoretical calibration graphs by computing digital holograms of spheres using Lorentz-Mie theory as described above, and calculating the axial shift, Δz_{LM-RS}, between the height of the particle according to Rayleigh-Sommerfeld reconstruction Z_{RS}, and Lorentz-Mie fitting Z_{LM}, with different values of particle size and height above the focal plane. Since Lorentz-Mie fitting recovers exactly the input position of the particles, Rayleigh-Sommerfeld reconstruction of the simulated holograms reveals the effective focal length of the particle, $\Delta z_{LM-RS} = z_{LM} - z_{RS}$ [10]. Figure 1 shows the measured Δz_{LM-RS} value from computer-generated holograms of polystyrene spheres in TE buffer. The result indicates clearly that z_{RS} depends not only on the particle's size, but also on its height above the focal plane. It has already been proven [8] that minor deviations exist in the value of Δz_{LM-RS} when a diffusing particle changes its height above the focal plane. Figure 1(a), however, proves these deviations are minor only when small particles ($a_p \sim 0.5\,\mu m$) are taken into account and cannot be ignored for

#181894 - $15.00 USD Received 18 Dec 2012; revised 1 Mar 2013; accepted 5 Mar 2013; published 10 May 2013

larger particles. The reason for the increased error in axial position of particle location obtained by Rayleigh-Sommerfeld reconstruction can be explained by a simple argument. The diffraction from each particle results in a pattern of rings with different locations and intensities, the most accurate reconstruction would use all diffraction rings. However, practical consideration limit the number of diffraction rings used for reconstruction, such as experimental optical noise obscuring the weaker rings, or the limited field of view chosen around the particle center for reconstruction. As a result, if too few diffraction rings are used a systematic error in location is created. From our simulations we can asses at which condition this systematic error can be avoided, and at which conditions a linear correction can be applied to correctly asses relative motion in the axial direction. It is important to state that the Lorentz-Mie fitting approach is more robust, since it can converge even when a smaller number of diffraction rings are fitted. To determine a range within which Rayleigh-Sommerfeld reconstruction is accurate at an experimentally available field-of-view we calculated Δz_{LM-RS} as a function of window size for different particle heights (see Fig. 1(b)). From Fig. 1 we learn that window size should be over 30 μm to reach a linear shift for particles between $a_p \sim 0.5-1$ μm, which we used for our experimental data reconstruction. For small particles ($a_p \sim 0.5$ μm), in standard imaging conditions, axial position obtained by Rayleigh-Sommerfeld reconstruction is insensitive to the distance from the microscope's focal length, at window sizes greater than 20 μm. Moreover, the accurate axial position of such a bead is about 0.8 μm above the bright feature in the rendered three dimensional image. In this way, we can produce height calibration curves for any given particle with known composition and size.

3.2. Experimental calibration

To test our calibration method we assembled an in-line holographic imaging microscope equipped with holographic optical tweezers (HOTs) [14]. Figure 2 shows a schematic representation of the integrated system, which is based on an inverted optical microscope (Olympus IX71) working at a magnification of 100*x* with an oil immersion objective lens ($NA = 1.4$). This lens is used both to project holographic optical traps, and also to collect in-line holographic images of trapped objects. Holographic traps are powered by a CW Ti:Shapire laser (Coherent) operating at a wavelength of 750 *nm*. The collimated laser light is imprinted with a phase pattern by a liquid crystal spatial light modulator (SLM, Hamamatsu X-10468-07) encoding optical trap location in the sample plane. Holographic imaging is achieved by illuminating the sample with laser light at 532 *nm* (DPSS, Coherent) and filtering out the trapping laser light. A CMOS camera (Gazelle, Point Grey Research) records the holographic images at a rate of 70 fps. Polystyrene colloids, $a_p = 1.025$ μm, were trapped at three different heights and allowed to diffuse within the trap. Trap height was measured in three techniques: by volumetric imaging of the light on a reflecting mirror [15], by Rayleigh-Sommerfeld reconstruction, and by fitting to Lorentz-Mie theory. Figure 3(a) shows the trajectory of the particle according to Lorentz-Mie fitting (blue dots), the average height according to Lorentz-Mie fitting (black line), z_{LM}, the average height according to Rayleigh-Sommerfeld reconstruction (red line, no calibration, no deconvolution), z_{RS}, and the height according to the volumetric imaging of the beam (green line), z_{mirror}. The shift between the axial position of the trap according to Lorentz-Mie fitting and volumetric imaging, changes with depth, and depends on the error in the assessment of the objective's focal length by volumetric imaging and on spherical abberations due to refractive index mismatch between the glass slide and TE buffer. The shift between z_{LM}, and z_{RS} is indeed not constant even for a displacement of 0.3 μm, however, z_{LM}, and z_{RS} are linearly dependent in this range (see Fig. 3(b)). The distribution of $z_{LM-RS} - < z_{LM-RS} >$ shown in Fig. 3(c) indicates that without calibration and deconvolution Rayleigh-Sommerfeld reconstruction has an axial positioning accuracy of about 55 *nm*. In order to use numerically obtained calibration data, we

#181894 - $15.00 USD Received 18 Dec 2012; revised 1 Mar 2013; accepted 5 Mar 2013; published 10 May 2013

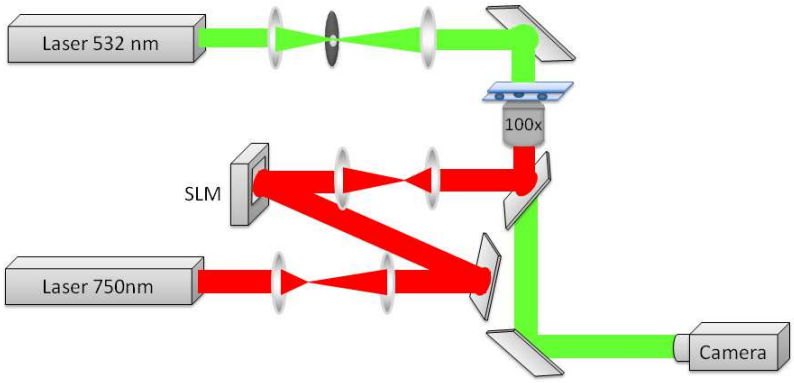

Fig. 2. Digital holographic microscope (green) combined with holographic optical trapping (HOT) [14] (red). A collimated laser beam (532nm) is expanded to overfill the field of view of a 100x objective lens of an Olympus IX71 microscope instead of its convention bright field illumination. A second laser beam (750nm) is expanded to overfill the face of a special light modulator (SLM) and relayed to the back focal plane of the same objective lens. The light pattern imprinted on the beam by the SLM focuses in the sample plane to form optical traps.

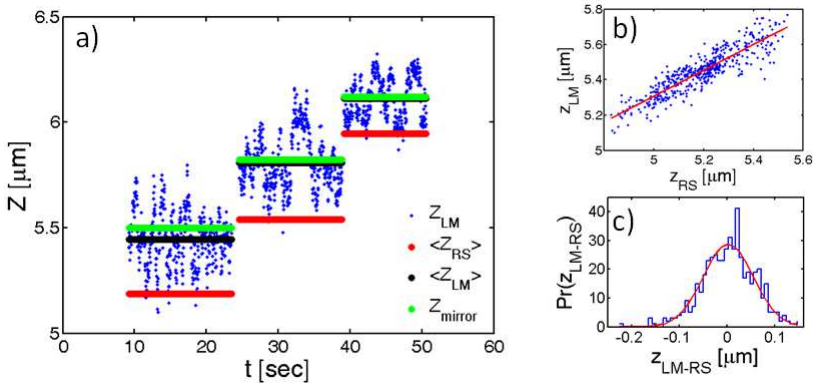

Fig. 3. Tracking results of a Polystyrene particle, $a_p = 1.025\mu m$, trapped with holographic optical tweezers at different heights. (a) Particle trajectory (Lorentz-Mie fitting (blue dots)), average height (Lorentz-Mie fitting (black line)), average height (Rayleigh-Sommerfeld reconstruction (red line), height by volumetric imaging (green line). (b) Correlation between z_{LM} and z_{RS} in the lowest trap. (c) Distribution of residuals after correction for systematic difference between z_{LM} and z_{RS} in the lowest trap.

wish to determine the parameter range in which it coincides with experiment. Specifically, for known particle size and sample composition we would like to compare the linear relation between z_{LM}, and z_{RS} (as measured in Fig. 3(b)), to an equivalent, numerically obtained, curve. To this end we performed a set of experiments tracking the diffusion of colloidal particles, creating calibration curves for them at two different heights and comparing them to numerically reconstructed calibration curves (Fig. 4). Theory and experiment agree well (Fig. 4(a)) at conditions in which simulations showed no dependence on window size, as the number of diffraction rings in the field-of-view decreases, a shift between simulation and experiment is observed (Fig.

#181894 - $15.00 USD Received 18 Dec 2012; revised 1 Mar 2013; accepted 5 Mar 2013; published 10 May 2013

4(b)). This shift remains constant for a range of at least 4 μm. In this range, therefore, numerical calibration curves suffice for determining the motion on the axial direction. Below we describe two experiment to which we applied our numerical calibration scheme.

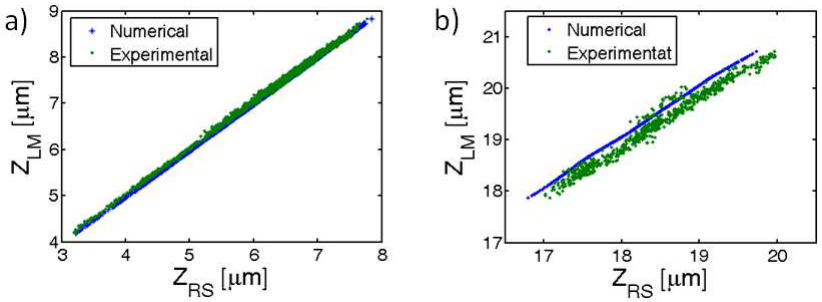

Fig. 4. Comparing numerical and experimental calibration of Rayleigh-Sommerfeld reconstruction against Lorentz-Mie (LM) fitting. Polystyrene colloids, $a_p = 0.55\ \mu m$, diffusing in TE buffer close (a) and far (b) from the microscope objective's focal plane.

4. Application to experiments

4.1. A particle diffusing near a wall

A single silica bead, suspended in an aqueous solution sediments to the sample cell floor due to gravity. It is repelled from the floor due to screened Coulomb interactions enhanced by plasma etching of the sample chamber. The height distribution of the sphere should be dominated at low heights by a sharp repulsion from the wall and decay exponentially as mgh/k_BT far from the wall [16]:

$$\begin{aligned} Pr(z) &= e^{\frac{E_{grav}+E_{elect}}{K_BT}} \\ \frac{E_{grav}+E_{elect}}{K_BT} &= -\frac{4\pi a_p^3 \Delta\rho g}{3k_BT} z - \frac{Q^2 e^{-\kappa}}{\varepsilon\kappa^2 a_p^3}(z-a_p) \end{aligned} \tag{10}$$

were $\Delta\rho$ is the difference between the density of silica and water, g is gravitational acceleration, Q is the effective charge on a charged particle, and κ is the Debye screening length. We followed the diffusion of such a silica bead ($a_p = 0.75 \pm 0.04\ \mu m$, Polysciences Inc.) as it floats above the glass floor Fig. 5. The trajectory of the particle was extracted using both reconstruction algorithms, applying the numerical calibration protocol to data from Rayleigh-Sommerfeld reconstruction (Fig. 5(a)). Having a glass wall near the diffusing particle distorts the diffraction pattern to some extent preventing the Lorent-Mie algorithms from correct convergence occasionally (see deviating green dots on Fig. 5(a)). While there is a small shift observed between the axial position according to both algorithms the height distributions coincide, well fitted by theoretical prediction (Fig. 5(b)), with $T \approx 28^oC$, $\kappa \approx 60nm$, and $Q = q(\kappa a_p)/(1+\kappa a_p)$ with $q \approx 6500$. For such application, where relative axial position is of interest, and boundary conditions distort the diffraction pattern, the calibrated Rayleigh-Sommerfeld reconstruction provides better reconstruction than the more elaborated Lorentz-Mie algorithm. This can be seen in two ways, the precision of particle positioning, which is extracted from the intercept of the mean square displacement plot [12] is comprable for both algorithms ($\varepsilon_{xy,RS} = \varepsilon_{xy,LM} \sim 1nm, \varepsilon_{z,RS} \sim 2.5nm < \varepsilon_{z,LM} \sim 3.5nm$), and the Lorent-Mie algorithm results in locations below the glass wall, ocationally (see low green dots, Fig. 5(a)). Our

#181894 - $15.00 USD Received 18 Dec 2012; revised 1 Mar 2013; accepted 5 Mar 2013; published 10 May 2013

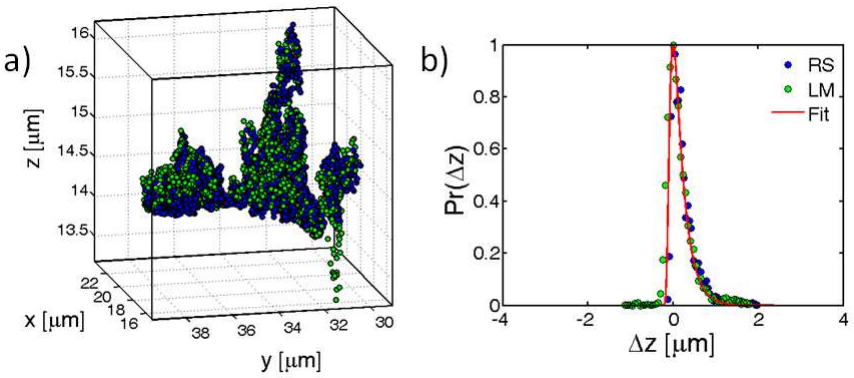

Fig. 5. (a) Trajectory of a silica bead suspended in water and floating above a glass floor extracted by Lorentz-Mie fitting (green) and numerically calibrated Rayleigh-Sommerfeld reconstruction (blue). (b) The height probability distribution of the sphere extracted by both methods and shifted so that the maximal values coincide, and confirm theoretical prediction.

goal however, is to use calibrated Rayleigh-Sommerfeld reconstruction to measure accurately axial positions of dense suspensions. To this end we must be able to measure the distance between two attached beads.

4.2. Two diffusing spheres

The main purpose of this study was to devise a method in which particle tracking in dense suspensions including aggregated particles could be done in 3D by in-line holographic imaging, with reliable and accurate positioning. The most challenging problem is to extract accurate location and distances between two attached particles of different size with highly overlapping diffraction patterns. To this end we created dilute suspension of colloidal particle pairs with different sizes, one with DNA coating and the other without. Our protocol involved mixing two suspensions, DIG-labeled 2 μm diameter (Spherotech) and NeutrAvidin-labeled 1 μm diameter (Invitrogen) Polystyrene spheres. Prior to mixing each suspension was diluted and washed three times by resuspension in TE buffer, centrifugation, and removal of the supernatant. The first set of experiments was performed after the two suspension were mixed and allowed to form aggregates. For the second set of experiments each suspension was incubated with λ-DNA (Invitrogrn) after washing and prior to mixing. In all experiments the resulting dilute suspension consisted of aggregates of colloidal particles from both sizes, we chose six particle pairs of each batch and imaged them holographically while diffusing in three dimensions. Using deconvolution Rayleigh-Sommerfeld reconstruction we measured the center-to-center distance between particle pairs and averaged over all measured pairs. In Fig. 6 the probability distribution of this distance during acquisition is plotted before and after the use of our numerical calibration scheme. In the absence of DNA we expect the inter-particle distance to be $d = 1.5\ \mu m$. Raw data show a wide distribution of distances due to the large difference in the effective focal length of the large and small particles, and due to its different dependence on height. However, after calibration the distribution collapses to a thin gaussian distribution centered around the expected value, $d = 1.505 \pm 0.038\ \mu m$. Suspension prepared with DNA show similar results, however a layer of approximately 100 *nm* is now coating each sphere.

#181894 - $15.00 USD Received 18 Dec 2012; revised 1 Mar 2013; accepted 5 Mar 2013; published 10 May 2013

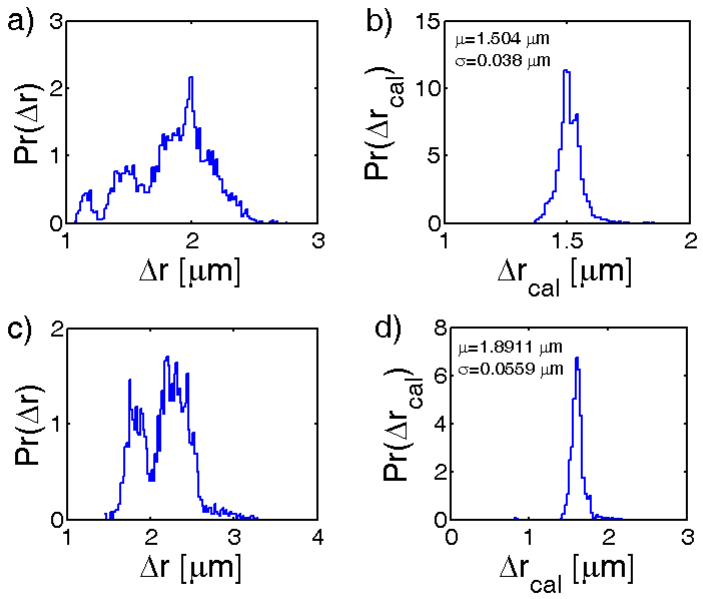

Fig. 6. Center-to-center distance (3D) between a 1 μm and a 2 μm diameter polystyrene attached beads diffusing in water, extracted from their Rayleigh-Sommerfeld reconstructed trajectories. Washed particles without (a) and with (b) calibration. DNA coated particles without (c) and with (d) calibration.

5. Conclusion

The flexible algorithm of hologram reconstruction based on Rayleigh-Sommerfeld back propagation can be transformed into an accurate measuring technique by use of the numerical calibration we introduced here. Our approach results in axial localization accuracy of the order of $40-60$ *nm*. As a result we were able to perform accurate three dimensional imaging at conditions which are challenging for the more accurate Lorentz-Mie algorithm, such as particles at the vicinity of scattering boundaries and for two attached particles with strongly overlapping diffraction patterns. Our calibration scheme opens new possible applications for in-line holographic imaging which will benefit from its capability for fast three dimensional imaging. For example, characterization of complex flow patterns in three dimensions, especially in microfluidic setups in which the scattering effect of the walls can be significant.

Acknowledgments

This work was supported in part by the James Franck German-Israeli Binational Program in Laser-Matter interactions, in part by the Marie Curie Reintegration Grant (PIRG04-GA-2008-239378), and in part by the Israel Science Foundation (Grants Number 1271/08).

#181894 - $15.00 USD Received 18 Dec 2012; revised 1 Mar 2013; accepted 5 Mar 2013; published 10 May 2013